

Dirac, Anderson, and Goldstone on the Kagomé

M. B. Hastings

Physics Department, Jadwin Hall

Princeton, NJ 08544

hastings@feynman.princeton.edu

We show that there exists a long-range RVB state for the kagomé lattice spin-1/2 Heisenberg antiferromagnet for which the spinons have a massless Dirac spectrum. By considering various perturbations of the RVB state which give mass to the fermions by breaking a symmetry, we are able to describe a wide-ranging class of known states on the kagomé lattice, including spin-Peierls solid and chiral spin liquid states. Using an RG treatment of fluctuations about the RVB state, we propose yet a different symmetry breaking pattern and show how collective excitations about this state account for the gapless singlet modes seen experimentally and numerically. We make further comparison with numerics for Chern numbers, dimer-dimer correlation functions, the triplet gap, and other quantities. To accomplish these calculations, we propose a variant of the $SU(N)$ theory which enables us to include many of the effects of Gutzwiller projection at the mean-field level.

I. INTRODUCTION

The spin 1/2 Heisenberg antiferromagnet on the kagomé lattice is a good candidate for a two-dimensional quantum system with a spin disordered ground state [1]. While it appears that on square [2] and triangular [3–5] lattices an antiferromagnet will acquire Néel order, on the kagomé lattice strong numerical evidence has accumulated that the system is spin disordered, as seen by the existence of a gap to triplet excitations and through consideration of the spectra of finite size samples [6]. Numerically, one finds a continuum of low energy states below the triplet gap. The continuum of low energy excitations provides a great puzzle to theory in the absence of an obvious broken symmetry.

There are good experimental realizations of kagomé systems, despite the presence of additional couplings, including the jarosites and $SrCrGaO$. While in iron jarosites [7,8], these additional couplings produce long-range order, in deuterium jarosite [9] and $SrCrGaO$ [10] no long range order is seen. Additionally, in $SrCrGaO$ a quadratic specific heat and very weak field dependence of the specific heat [11] are in agreement with the picture of a continuum of low-energy singlet excitations seen in numerics, suggesting that the latter two compounds provide good realizations of the kagomé antiferromagnet.

Given the lack of spin order, RVB ideas seem natural for this system, and indeed have stimulated much theoretical work on the system. Large N calculations based on $SU(N)$ have been used to suggest a spin-Peierls state [12]. Calculations based on $Sp(2N)$ have suggested a phase with deconfined, gapped, bosonic spinons [13]. Chiral states have also been proposed [12], but do not account for the excitation spectrum and also are in disagreement with the rapid decay of chirality-chirality correlation functions seen in numerics. States with BCS pairing have been suggested but again do not account for the excitation spectrum; due to the non-bipartite nature of the kagomé lattice, these states are *not* equivalent to flux states [14]. In addition to the long-range states, short-range RVB states based on a reduced Hilbert space of dimers [15–17] have also been considered and provide some explanation for the gapless continuum.

An RVB state on the kagomé lattice would be particularly attractive, given the intensive work on RVB states on the square lattice [18], especially in connection with high- T_c materials [19]. In the absence of doping, the square magnet eventually acquires Néel order and the spinon excitations disappear from the system. Since the kagomé lattice does not acquire Néel order, it could be a very important model for a spin liquid or spin solid state.

The idea behind the present approach is to start with a long-range RVB treatment of the kagomé lattice and consider various ways of gapping the spinon excitation spectrum. We will first construct a “parent state” which will be the best RVB state that does not break time-reversal symmetry or any lattice symmetry.

We will then demonstrate an interesting massless Dirac structure for this state. Various other known RVB states can be obtained by perturbing the parent state, lowering the symmetry and giving mass to the Dirac particles, so that the parent state unifies a wide class of states. Physically, we expect that the system will attempt to give mass to the Dirac particles and open a gap, picking out one of these other lower symmetry states. We will discuss the symmetry breaking through a renormalization group treatment. We will obtain some kind of spin solid state, and some low energy Goldstone and gauge excitations, which we will argue provide the low energy degrees of freedom seen experimentally.

The RVB states can be thought of by a decoupling procedure, in which we decompose spin-1 operators into pairs of spin-1/2 operators. Take a Hamiltonian

$$H = \sum_{\langle i,j \rangle} 2J \vec{S}_i \cdot \vec{S}_j \quad (1)$$

where the sum extends over neighboring sites i, j . We use an unconventional normalization of J to agree with the definition of Waldtmann et. al. [20], and to simplify equation (2) below.

Introduce the spinon fields $\psi_a^\dagger(i), \psi_a(i)$, where $a = u, d$ labels up and down spinon fields. We can then introduce a Hubbard-Stratonovich field $t_{ij} = t_{ji}^\dagger$ such that

$$H = \sum_{\langle i,j \rangle} \left(\psi_a^\dagger(i) t_{ij} \psi_a(j) + h.c. \right) + \frac{1}{J} \sum_{\langle i,j \rangle} |t_{ij}|^2 \quad (2)$$

By taking a mean-field in t , minimizing the total energy of the fermions and the Hubbard-Stratonovich field, we obtain an RVB state. One must at some point project results onto the physical space in which each site is singly occupied.

Later, we will find this projection to be extremely important. In the absence of projection, the ideal mean-field state is almost always found by taking a dimer covering of the lattice [21], with t_{ij} nonvanishing only on the given dimers. Projection can stabilize RVB states, so although our first calculations will ignore the effects of projection, in a naive mean-field, we will later discuss a projected mean-field that includes some of the essential effects of projection.

We will then have to proceed beyond mean-field solutions. We will consider a functional integral with fields $\psi(i)$ and t_{ij} , fluctuating about a saddle-point of the action. There are a large number of possible fluctuations in t_{ij} , including a set of pure gauge fluctuations, as well as a set of gauge fields. Most other fluctuations can be ignored because they do not contribute to the low-energy dynamics. However, there will be a particular set of fluctuations in t_{ij} that produce a mass for the fermion field. Although these fluctuations are not gapless, we will retain these fluctuations due to their impact on the low energy dynamics of the fermion field. We will see using a renormalization group that the effective action of these fields can differ greatly from that suggested by the mean-field.

To outline the paper, we will first describe the parent state, and then discuss how to perturb the parent state to obtain other proposed RVB states. Then we will discuss naive and projected mean-field theory treatments of these states. We will then proceed to a field theoretic treatment of fluctuations about the mean-field and a renormalization group that will suggest one particular symmetry breaking pattern. We will discuss the pseudo-Goldstone and gauge modes that arise from this symmetry breaking, and the mechanism that ultimately gives them a very small energy gap.

Next, we proceed to a discussion of finite system size effects as a first step in comparison with numerics. These effects lead to an additional flux for odd system sizes which leads to a nonvanishing Chern number for odd system sizes. We will then compare the low energy bosonic modes from the field theory to the low energy singlet modes found in numerical calculations as well as checking dimer-dimer correlation functions and many-body density of states.

II. THE PARENT RVB STATE

Although the short range RVB calculations provide one starting point for the kagomé lattice antiferromagnet, we will be interested in looking at long range states instead. Certainly, the short range RVB calculations themselves suggest that long range antiferromagnetic correlations are important; the variational energy of these states improve when second neighbor dimers are included. Further, while the kagomé lattice has a gap to triplet excitations, this gap is about an order of magnitude smaller than J ; from a short range calculation one might expect a gap of order J as that is the energy to break a dimer. However, Mila has suggested that within a short-range state it is possible to have a triplet gap much smaller than J [17], so the small triplet gap does not necessarily rule against a short-range state.

The best RVB state on the kagomé lattice antiferromagnet is a chiral spin liquid [12]. A similar chiral state [22] was obtained using a hardcore boson representation of the spins and transmuting the statistics from bosonic to fermionic using a Chern-Simons field. However, numerical calculations [20] do not support a large chirality-chirality correlation function or expectation value of the chirality operator, which would seem to rule these states out. So, we will look for the best RVB state that is not chiral.

Assuming that we are looking for a long-range RVB state in which all t_{ij} have the same magnitude, the only choice we have is how much flux to put into the system. The state we choose involves putting π flux through the hexagons, and no flux through the triangles. This state offers a better mean field energy than any other nonchiral RVB state, including the state with no flux through the system at all.

The unit cell of the kagomé lattice consists of three sites on a triangle. Once we add flux to the system, the unit cell doubles, and requires six sites on two triangles. We will find it convenient to double the unit cell again, to twelve sites, including six sites on a hexagon and the six sites which neighbor the hexagon. This cell is shown in figure 1.

The kagomé lattice is made up of a triangular lattice of these 12-site unit cells. We have numbered the points in the cell for later reference.

For now, let us assume that we pick J such that $|t| = 1$ within our RVB state. Then, the band structure for our RVB state is shown in figure 2 scanning along the given line of momenta in the Brillouin zone. There is a degeneracy of states: the bottom line in the figure actually consists of four bands, while the other four lines in the figure consist of two bands each, providing a total of twelve bands. At $(0,0)$, four bands meet at energy less than zero and another four meet at positive energy. Near this point the spectrum becomes relativistic.

The particles occupy the lowest six bands of the system, meaning that where the bands meet the spectrum becomes gapless. The system can gain energy by perturbing about our given RVB state; we expect that the greatest gain in energy comes from opening a gap. For this reason, we will study the Dirac point and look at possible perturbations to the Dirac equation.

At the Dirac point, the Schrödinger equation for the fermions becomes

$$E\psi = v_f(\alpha_x k_x + \alpha_y k_y)\psi \quad (3)$$

where ψ is a four component spinor, and the matrices α_x, α_y are anti-commuting α -matrices. The particular basis chosen for ψ and for the α -matrices is unimportant. We find by explicit computation that

$$v_f = (0.408248\dots)|t| \quad (4)$$

Given the Dirac equation (3), we would like to consider the effect of perturbations δt_{ij} on the low energy structure. This analysis will enable us to focus on those fluctuations in t_{ij} which have the greatest impact on the low-energy dynamics and which must be kept when we proceed to a field-theory treatment of fluctuations.

From equation (2), the system pays an energy cost equal to $\frac{1}{J}|\delta t_{ij}|^2$, but it can gain energy by opening a gap for the Dirac particles. As a result, we look for the perturbations which open the greatest gap for the Dirac particles for given $|\delta t_{ij}|^2$. Let us first proceed algebraically, considering possible perturbations to the Dirac equation which will open a gap, and only then ask how to obtain these perturbations from δt_{ij} .

A given perturbation δt_{ij} will perturb the Dirac equation to

$$E\psi = \left(v_f(\alpha_x k_x + \alpha_y k_y) + M\right)\psi \quad (5)$$

where M is some matrix, the projection of δt_{ij} onto the space of the four states at the Dirac point. It may be shown that the perturbation M will be most efficient at opening a gap when it anti-commutes with α_x, α_y . By efficient, we mean that we wish to maximize the gap for given $\text{Tr}(M^2)$, as a first step to maximizing the gap for given $|\delta t_{ij}|^2$. Since there is only a sixteen dimensional space of matrices M , we can easily characterize all matrices that have the needed anti-commutation property; it is a four dimensional vector space.

We will write three of the perturbations as matrices M_i , for $i=1,2,3$. In terms of α -matrices, they will be $M_1 = \alpha_z, M_2 = \beta, M_3 = \beta\alpha_x\alpha_y\alpha_z$. These perturbations anti-commute with each other; in fact, one can make a change in basis in the Dirac equation which leaves α_x, α_y unchanged, but produces continuous $O(3)$ rotations in the space of M_1, M_2, M_3 . This continuous symmetry is only valid at low energy; it will be broken to a discrete symmetry by lattice effects as discussed below. By taking $M = \sum_i m_i M_i$, for some numbers m_1, m_2, m_3 , we open a gap equal to $\sqrt{\sum_i (m_i^2)}$. We will refer to these as nonchiral mass terms.

The fourth perturbation is of a different sort. It is $M = m_c M_c$ with $M_c = i\alpha_x\alpha_y$ (here, c stands for chiral and we will refer to this as a chiral mass term). This perturbation breaks parity and time-reversal symmetry. M_c commutes with M_1, M_2, M_3 . As mentioned above, we are interested in the most efficient way for the system to open a gap; since M_c does not anti-commute with M_i , it is most efficient for the system to take either purely chiral mass or purely nonchiral mass, so that $m_i = 0$ or $m_c = 0$.

Next, we would like to ask what perturbations in the t_{ij} will produce the desired mass matrix M . We will find that to produce M_i requires dimerizing the system by making the magnitudes of the $|t_{ij}|$ non-uniform; to produce M_c requires adding additional fluxes to the system. Clearly, there is a large degeneracy here, as there is a only 16 dimensional space of matrices M while in a given unit cell there is a 48 dimensional space of perturbations to t_{ij} . While some of the degeneracy is due to the large number of possible gauge transforms on t_{ij} , this does not completely alleviate the problem. Again, the question of efficiency becomes important: for each M , there is a class of t_{ij} which produce the desired perturbation, but only one element in the class minimizes $\sum_{i,j} |t_{ij}|^2$. We will find one unique perturbation in t_{ij} (up to arbitrariness in gauge) which produces the desired mass matrix.

The perturbation that we will pick for M_1 is shown in figure 3. One can see that all the horizontal bonds have been either decreased or increased in strength, such that along a horizontal line the bonds alternate in strength while horizontal bonds which are in a vertical column all have the same strength.

This perturbation is a dimerization of the t_{ij} . The spins form singlets most strongly across the largest t_{ij} , so that dimerization of t_{ij} tends to produce a spin solid and changes the long-range RVB to a short range set of singlets.

This mass term breaks rotational and translational symmetry of the lattice. We will pick M_2 and M_3 to be lattice rotations of M_1 . The continuous symmetry of the Dirac equation will then be broken at the lattice level to a discrete symmetry of permutations of m_1, m_2, m_3 under lattice rotation, while lattice translations change the sign of any 2 of the 3 mass terms m_1, m_2, m_3 . We will find later that while we obtain symmetry breaking and produce a mass, the discrete nature of the lattice group will leave us with only pseudo-Goldstone modes.

There are two mass terms which are symmetric under rotations. They are

$$M_{12} = \frac{M_1 + M_2 + M_3}{\sqrt{3}} \quad (6)$$

$$M_6 = -M_{12} = \frac{-M_1 - M_2 - M_3}{\sqrt{3}} \quad (7)$$

where 12 denotes the fact that the t_{ij} are strongest on the 12-site loop surrounding the unit cell, while 6 denotes the fact that the bonds are strongest on the hexagons and triangles. We show the perturbation to t_{ij} to produce M_{12} in figure 4.

To estimate dimerization later, it will be useful to know connect the change in t to the eigenvalues of the mass matrix that arises. One finds that if the bonds on the 12-site loop are increased by δt , while those on the hexagons and triangles are decreased by the same amount, then one produces a term $m_{12}M_{12}$ in the Dirac equation with $m_{12} = 1.57735\dots\delta t$.

For calculations later, it will be convenient to transform to a basis of gamma matrices. Defining $\gamma_t = \beta$, $\gamma_i = \beta\alpha_i$, we find that $M_1 = \gamma_3$, $M_2 = 1$, $M_3 = i\gamma_5$, while $M_c = i\gamma_t\gamma_x\gamma_y$.

It is interesting to compare to above characterization of possible perturbations in terms of gamma matrices to the situation in the π -flux phase on the square lattice, where there is again a Dirac spectrum. We find that we are able to introduce one nonchiral mass term by dimerizing the horizontal bonds of the square lattice, so that the horizontal bonds alternate in strength as one moves horizontally along the lattice; another mass term can be introduced by dimerizing the vertical bonds. In the limit of extreme dimerization, these states correspond to short-range RVB states in which the dimers are stacked on top of each other, and all lie either horizontally or vertically [23]. By taking sums of these two mass terms, we can produce a short range state in which dimers resonate around a square. The final nonchiral mass term can be obtained by placing an on-site potential on one sublattice of the square lattice; this corresponds to introducing Néel order into the system [24]. Due to the highly frustrated nature of the kagomé lattice, we will not have such any terms involving introducing on-site potentials.

For the square lattice, the chiral mass term can also be introduced. It requires adding additional couplings to the system, which connect diagonally across a given plaquette, and then inserting $\pi/2$ flux through the triangle that is formed when a particle traverses two sides of a plaquette and then crosses the plaquette on the diagonal [25].

III. CONNECTION TO OTHER VALENCE BOND STATES

From the parent state, it is possible to continuously connect to other possible valence bond states, using the mass terms we have found above. Let us first consider the chiral spin liquid and then the spin-Peierls solid of Marston and Zeng [12].

Let us consider a state such that the flux through each triangle is equal to θ , and the flux through each hexagon is equal to $\pi - 2\theta$. Then, as θ varies from 0 to $\frac{\pi}{2}$ we continuously deform from the parent state to the chiral spin liquid. By looking at how t_{ij} changes along this deformation, and then projecting this change onto the Dirac point, we find that for small θ , the perturbation exactly produces the chiral mass term M_c ! Let us note that at $\theta = \frac{\pi}{4}$ there is a highly interesting band structure, discussed in the Appendix, with multiple flat bands.

The chiral spin liquid state improves on our parent state at the mean-field level. Since we will argue below that fluctuations stabilize our state against the chiral mass term, let us here analyze why the chiral state works at the mean-field level, and provide a qualitative explanation of why fluctuations destroy the chiral spin liquid.

The idea behind the chiral state results from the ‘‘Rokhsar rules’’ [26], which argue that one should put flux $\frac{\pi}{2}$ through every triangle, no flux through the hexagons, and have a total flux of π through the loop of length twelve that surrounds a hexagon and its six attached triangles. These rules are derived from considering individual hexagons and triangles in isolation, and minimizing the mean-field energy.

While our parent state appears to violate every one of the rules, except the rule for the length-12 loop, the chiral spin liquid is in perfect agreement with these rules! Let us focus on one isolated triangle, with $|t| = 1$. If there is

no flux through the triangle, there are two negative energy states with energy -1 . We can put two particles in one state, and one in another, for a total energy of -3 . By adding $\frac{\pi}{2}$ flux, we have one state at energy $-\sqrt{3}$ and another state at energy zero. By putting two particles in the lowest energy state, we improve the energy of the system, and introduce a chirality.

Now, consider the triangle coupled to the rest of the system. If the rest of the system strongly scatters the particles in the triangle, it may no longer be appropriate to think of two particles in one state and one in another. One must instead think of each of the two negative energy states of the triangle as each having average occupation of one-and-a-half particles. In that case, it is most advantageous to put no flux through the triangle.

So, if the system to which the triangle is coupled is chiral, so that all triangles in the system have the same flux $\frac{\pi}{2}$, then the chiral spin liquid may work. But if the triangle is coupled to states which are not chiral, then the chiral spin liquid is destroyed. One sees this even at the mean field level; a state in which triangles have alternating flux $\pm\frac{\pi}{2}$ is significantly worse in energy than our parent state. Similarly, if one introduces sufficiently strong dimerization m_{12} , one finds that the system is stable against weak m_c . Within the RG below, we will consider the fluctuations in the masses m_i and show that they help stabilize the parent state against the chiral perturbation.

The spin solid of Marston and Zeng can also be obtained from the parent state. In this spin solid state, the idea is to look for dimer coverings which maximize the number of “perfect hexagons”, hexagons on which three of the bonds are covered by dimers. Attached to these hexagons are “defect triangles”, triangles on which no bonds are covered by dimers. Clearly, we wish to increase $|t_{ij}|$ on the perfect hexagons, while decreasing it on the defect triangles. This will project onto the mass term M_6 on the 12-site cell that includes the given perfect hexagon.

The perfect hexagons are then supposed to form a lattice. We can obtain this lattice by taking the triangular lattice of 12-site cells, and placing perfect hexagons inside the 12-site cells on two out of the three sublattices of the triangular lattice. In this case the cells containing perfect hexagons form a honeycomb lattice. This gives rise to a staggered mass state. We produce a mass term M_6 on two-thirds of the system, so that the Dirac particles feel a net M_6 at zero momentum, as well as a fluctuating M_6 at finite momentum.

IV. NAIVE MEAN-FIELD AND PROJECTED MEAN-FIELD

To compare the energies of possible RVB states, including the various mass perturbations of our parent state, we turn to the RVB mean field. When we look for a mean-field solution of t_{ij} in equation (2), it is known [21] that the best mean-field is a dimer covering. Still, let us start by looking at results of the naive mean-field calculation, and then later provide a projected mean field calculation.

Let us introduce the Green’s function between sites, G_{ij} , defined to be the sum over all occupied fermionic states, ψ , of

$$\psi^\dagger(i)\psi(j) \tag{8}$$

The fermionic energy is then equal to

$$\sum_{\langle i,j \rangle} G_{ij}t_{ji} \tag{9}$$

For our parent state, explicit calculation shows that, for nearest neighbors i, j ,

$$|G_{ij}| = 0.221383... \tag{10}$$

From the mean-field condition for equation (2), we find for the parent state that $t = 0.221383J$, so by equation (4)

$$v_f = (0.0904...)J \tag{11}$$

We find that within the projected mean-field that the parent stable is unstable to all of the massive fluctuations, including the chiral mass fluctuation which will drive the system to a chiral spin liquid.

For infinitesimal perturbations, the different nonchiral masses all provide an equivalent improvement in mean-field energy. To some extent this is due to the approximate low energy symmetry of the Dirac equation to rotating continuously among the different mass terms. However, it is interesting that lattice effects do not break this symmetry. The reason is the discrete lattice symmetry. The change in energy for taking $M = m_1M_1 + m_2M_2 + m_3M_3$ is, for small m , a quadratic form in m_i . Let this form be

$$\sum_{i,j} c_{ij}m_im_j \tag{12}$$

The coefficients c_{11}, c_{22}, c_{33} in this form must all be the same due to lattice rotation symmetry. Lattice translation symmetry permits one to change the sign of any two of the m_i , and prevents a nonvanishing c_{ij} for $i \neq j$. Therefore, for small perturbations the energy gain for introducing a mass must be dependent only on the magnitude of the mass, not the particular mass term used. For larger perturbations, the energy gains may depend on the particular mass term used, and of all the nonchiral mass terms, the system gains the most energy by a mass M_{12} .

Now let us turn to the projected mean-field. Instead of doing a full Gutzwiller projection, we will use an approximation introduced by Hsu [24]. Within a variational Gutzwiller projection, one minimizes the energy of the Hamiltonian (1). Hsu's idea at the lowest level of approximation is to note that the Hamiltonian is a sum of terms $J\vec{S}_i \cdot \vec{S}_j$ over different neighbors i, j , and, when evaluating the expectation value of each of these terms, to perform the projection only on the given sites i, j . At this level, the variational principle corresponds to minimizing

$$\sum_{\langle i,j \rangle} (\vec{S}_i \cdot \vec{S}_j) \approx - \sum_{\langle i,j \rangle} 6 \frac{|G_{ij}|^2}{1 + 16|G_{ij}|^4} \quad (13)$$

over all possible t_{ij} , where G_{ij} is determined by t_{ij} .

For our parent state, we find that $-6 \frac{|G_{ij}|^2}{1+16|G_{ij}|^4} = -0.2832\dots$ By going to the chiral spin liquid, the system improves the ground state energy by roughly 2.9 percent within the projected mean-field approximation. By going to a state with staggered $\pm \frac{\pi}{2}$ flux through each triangle, the system worsens the ground state energy by roughly 1.4 percent. Within this approximation the system is stable against the nonchiral mass perturbations as all the nonchiral mass perturbations worsen the ground state energy at this level of approximation. Again due to discrete lattice symmetry, the energy cost is independent of the particular mass term for small mass, while for larger perturbations, the energy costs differ, and the M_{12} perturbation costs the least energy.

V. FIELD THEORY OF FLUCTUATIONS

Having discussed the naive and projected mean-fields for the problem, we must include fluctuations about the mean-field. To do this, we will use an $SU(N)$ generalization of the original problem [27], such that the projection procedure of Hsu becomes exact. After discussing how to do this in the abstract, we will present the field theory for our specific problem: it will have a number of interacting fields, including fermions, gauge fields, the nonchiral mass terms discussed above, which we will refer to as "pion" fields, and the chiral mass term.

The approximation of Hsu amounts to minimizing equation (13). By introducing an auxiliary field λ_{ij} we can "decouple" this sum of functions of G_{ij} and instead extremize the function

$$\sum_{i,j} G_{ij} \lambda_{ji} + f(|\lambda_{ij}|^2) \quad (14)$$

where $f(|\lambda|^2)$ is a Legendre transform of $\frac{|G|^2}{1+16|G|^4}$.

Then, we can interchange the order of extremizations, and extremize this quantity over t_{ij} before extremizing over λ_{ij} . We find that this is extremized at $t_{ij} = \lambda_{ij}$. Then we proceed to extremizing over the one remaining set of variables λ_{ij} . But since $t_{ij} = \lambda_{ij}$, we are equivalently trying to extremize the function

$$\sum_{i,j} G_{ij} t_{ji} + f(|t_{ij}|^2) \quad (15)$$

over all t_{ij} . Note, now, that $G_{ij} t_{ji}$ is exactly the kinetic energy of the fermions. So, finally, we are trying to extremize

$$H = \sum_{\langle i,j \rangle} \left(\psi_a^\dagger(i) t_{ij} \psi_a(j) + h.c. \right) + \sum_{\langle i,j \rangle} f(|t_{ij}|^2) \quad (16)$$

Returning to the language of functional integrals, we can introduce an $SU(N)$ field theory for which the Hsu projection procedure becomes exact. We take a large N limit in the number of fermion fields in equation (16), so that $a = 1\dots N$. Then, we integrate over all possible t_{ij} in that equation, undoing the decoupling procedure above, and rewrite the result in terms of spin operators. We find

$$H = \sum_{\langle i,j \rangle} \frac{\vec{S}_i \cdot \vec{S}_j}{1 + 16\vec{S}_i \cdot \vec{S}_j} \quad (17)$$

We should note a few facts about this procedure. When we demonstrate the equivalence of the large N mean-field with the Hsu mean-field, it is the large N limit that permits us to ignore fluctuations in t_{ij}, λ_{ij} , so that the decouplings amounts exactly to taking a Legendre transforms; at finite N , the decoupling of an interaction is not exactly a Legendre transform. Further, we used the word “extremize” above with care: in some cases we maximize while in other cases we minimize, as in some places the function $\frac{|G|^2}{1+16|G|^4}$ has positive curvature while in other cases it has negative curvature. This does not provide any formal problems when performing the decoupling at the level of functional integrals, so long as we correctly choose the integration contour of λ_{ij} .

The fractional operator, $\sum_{\langle i,j \rangle} \frac{\vec{S}_i \cdot \vec{S}_j}{1+16\vec{S}_i \cdot \vec{S}_j}$ in equation (17) may be interpreted as a formal power series, so that it includes operators of the form $(\vec{S}_i \cdot \vec{S}_j)^k$ for all k . At $N = 2$, this operator is equivalent to $\vec{S}_i \cdot \vec{S}_j$, up to a constant factor.

Finally, the above procedure is similar to the technique of introducing biquadratic interactions, $(\vec{S}_i \cdot \vec{S}_j)^2$, into the Hamiltonian to stabilize RVB states against dimerization. We simply prefer the above Hamiltonian as it reproduces exactly our desired mean-field theory.

Having defined a large N theory with no fluctuations in the decoupling fields, we next add in fluctuations. Formally, this can be handled by a $1/N$ expansion. We will directly write the field theory at $N = 1$ without including explicit factors of N .

The theory includes several modes. There is the Dirac fermion field, $\psi(x)$. This is coupled to a fluctuating $U(1)$ gauge field, $A^\mu(x)$, $\mu = t, x, y$. By considering other fluctuations in t_{ij} we will also obtain a fluctuating chiral mass field that we will refer to as $\sigma(x)$, and a triplet of fluctuating nonchiral mass terms that we will group into one “pion” field $\pi^a(x)$, $a = 1, 2, 3$. If the pion field acquires an expectation value, then the fermions will acquire a mass $m_a = \langle \pi^a \rangle$.

For the field theory, we will suppress the velocity v_f . At the level of the bare action the pi, sigma, and gauge fields can have different velocities from the fermi fields. However, the greatest contribution to the effective action of the bosonic fields arises from integrating over the relativistic fermions, so that at low energies the velocity of the bosonic fields must be roughly equal to that of the fermionic fields.

The Lagrangian L we will take is

$$L = \int d^3x L_f + L_A + L_M \quad (18)$$

where

$$L_f = \bar{\psi}_{u,d}(x) \left(\gamma^\mu (A_\mu + i\partial_\mu) + \gamma_0 M_a \pi^a + \gamma_0 M_c \sigma \right) \psi_{u,d}(x) \quad (19)$$

$$L_A = \frac{1}{4\Lambda g_a^2} F_{\mu\nu} F^{\mu\nu} \quad (20)$$

$$L_M = \frac{1}{2\Lambda g_\sigma^2} \sigma(x) \left(\partial_\mu^2 + m_\sigma^2 \right) \sigma(x) + \frac{1}{2\Lambda g_\pi^2} \pi^a(x) \left(\partial_\mu^2 + (m_\pi^2)^{ab} \right) \pi^b(x) \quad (21)$$

We have written the mass for the pion field as a matrix. However, following the arguments for equation (12), the masses of the different pion modes must be the same. It is only after condensation of the pion field, breaking the lattice symmetry, that the masses can differ.

We have inserted factors of Λ , representing a lattice cutoff scale, into the action to make the coupling constants dimensionless. We have chosen to scale the bosonic fields so that all coupling constant dependence appears in the action L_A and L_M , not L_f .

In addition to the terms we have written, there must be a quartic interaction term for the π and σ fields. This term is necessary to stabilize the action if the system spontaneously breaks a symmetry and has either $m_\pi < 0$ or $m_\sigma < 0$. Since we will be initially starting the renormalization group of the next section with both such masses positive, we can temporarily ignore the quartic term at high energy under the assumption that this term is small. If the system acquires an expectation value for the π fields, the quartic term will break the continuous symmetry down to the lattice symmetry, and give a small mass m_π^\perp for the approximate Goldstone modes. There will also be cubic terms that give a mass to these modes.

Another interesting term we have left out is $\bar{\psi} \gamma_\mu \gamma_\nu F^{\mu\nu} \psi$, which can be added to change the g -factor of the Dirac fermions. In the absence of external fields, there are two degenerate states of the Dirac equation at each energy. For physical electrons, this reflects a spin degeneracy. For the spinons we consider, which already have a definite spin, this

degeneracy instead reflects a *chirality* degeneracy, and we will refer to it as such. If the system has an odd number of sites, and hence an unpaired spinon, not only does the system have a net spinon, but it also has a net chirality, which can be taken to be positive or negative. Generically the g -factor will be non-zero.

VI. RENORMALIZATION GROUP

We will consider the one-loop RG from the field theory. We will see that it is indeed possible for fluctuations to lead to a condensation of the pion field.

For the gauge, pion, and sigma fields we will use a simple mode elimination RG, with a cutoff Λ . For the fermion fields, we will introduce a set of massive regulator fields with masses of order Λ and reduce the regulator mass. The choice of the particular mass terms for the regulator fields represents a lattice breaking of the Goldstone symmetry. It is possible to preserve the needed lattice symmetry of equation (12) by introducing seven regulator fields. Four are ghost fields with masses proportional to $M_1 + M_2 + M_3, M_1 - M_2 - M_3, -M_1 + M_2 - M_3, -M_1 - M_2 + M_3$ and the other three are not ghosts and have masses proportional to M_1, M_2, M_3 .

Initially the theory will have a cutoff Λ_0 , defining the lattice scale. As we renormalize, we lower the cutoff Λ , and rescale all distances and fields to keep Λ fixed.

We must take into account self-energy corrections to the fermions from interactions with the bosonic fields, vertex corrections, and self-energy corrections to the bosonic fields from vacuum polarization bubbles. If we were to take into account only the self-energy corrections to the bosonic fields, and not the vertex and fermionic self-energy terms, we would find that we are considering just the mean-field theory in the bosonic fields.

We find the following RG equations:

$$\frac{d\ln g_A}{d\ln(\Lambda_0/\Lambda)} = 1 - \frac{g_A^2}{3} \quad (22)$$

$$\frac{d\ln g_\pi}{d\ln(\Lambda_0/\Lambda)} = 1 + \frac{3g_A^2 + g_\pi^2 - g_\sigma^2}{2\pi^2} + \text{vacuum polarization} \quad (23)$$

$$\frac{d\ln g_\sigma}{d\ln(\Lambda_0/\Lambda)} = 1 + \frac{3g_A^2 - 3g_\pi^2 - g_\sigma^2}{2\pi^2} + \text{vacuum polarization} \quad (24)$$

$$\frac{dm_\pi^{ab}}{d\ln(\Lambda_0/\Lambda)} = 2 + \text{vacuum polarization} \quad (25)$$

$$\frac{dm_\sigma}{d\ln(\Lambda_0/\Lambda)} = 2 + \text{vacuum polarization} \quad (26)$$

We have avoided explicitly writing the vacuum polarization contributions to the sigma and pion fields. The vacuum polarization contribution to the mass is regularization dependent, while the vacuum polarization contribution to the coupling constant is ultraviolet convergent and is dominated by the infrared contribution.

Fluctuations in the gauge field increase the coupling constants for the pion and sigma fields. This reflects the binding force due to the gauge field between charged spinons, and the resulting tendency to break chiral symmetry. Further, we see that the coupling constant for the pion field increases more rapidly than that for the sigma field, reflecting the destabilization of the chiral state by fluctuations in the pion field.

Thus, we see from the renormalization group that there is a range of bare parameters such that the theory will condense the pion field, producing a nonchiral mass term for the fermions, even though at the mean-field level the theory would rather produce a nonchiral mass term for the fermions.

In the next section we will consider the low energy action after condensation. We will first discuss the mass term for the fermions that appears.

Unfortunately, it is beyond our ability to calculate the bare parameters in the field theory with any precision, and so the mass of the fermion field is not something we can compute. Let us instead take the mass of the fermion as an input from numerics, and use that to check for consistency of our theory. Extrapolating finite size results from systems of up to 36 sites, one finds that the system has a gap to triplet excitations which is of order $J/10$ or less [20]. While the gap is decreasing even at the largest sizes, it appears to be bounded below by roughly $J/20$. Assuming

that the triplet excitations are made of pairs of spinons, we can estimate the spinon gap as being half the triplet gap. Further evidence for the spinon gap being roughly half the triplet gap comes from odd-even studies of the energy dependence on N [20]. The fermion mass is half the spinon gap, or one quarter the triplet gap.

Using this estimated spinon gap, and the calculated velocity of our Dirac particles from RVB theory, we can obtain the correlation length of the Dirac particles. Taking the estimate of $J/10$ for the triplet gap, we find that the correlation length is roughly 4 of our twelve-site unit cells, large enough to include the $N = 36$ numerical studies.

We can also estimate the strength of dimerization at the mean field level, by asking how large a change in t_{ij} is needed to produce the desired mass term. Assuming that the dimerization is provided by a perturbation of the form M_{12} , one finds that the t_{ij} 12-site loops are increased by approximately 7 percent, while the other bonds are decreased by 7 percent. This is a relatively small amount of dimerization, and we expect that only after a significant increase in system size will numerical studies be able to detect this directly from a dimer-dimer correlation function.

VII. LOW ENERGY MODES

The remaining low energy modes after the pion field condenses are the Goldstone excitations of the pion field and the gauge excitations, which we will argue provide the low energy singlet modes seen in numerics. While numerical calculations have only probed systems up to $N = 36$ sites, which is relatively small considering that we take a unit cell of 12 sites, experiment also reveals a quadratic low temperature specific heat. This specific heat suggests that a bosonic mode with a linear density of states survives to much larger scales, while the insensitivity of the specific heat to weak magnetic fields suggests that the mode is still a singlet. In this section we will first discuss the nature of the low energy modes and then the ultimate fate of our pion and gauge excitations at large distances, including a gap for the pion from lattice effects as well as a confining phase for the gauge fields.

Once the pion field condenses, the system is left with two pseudo-Goldstone pion modes as well as gauge modes. The gauge action is

$$L_A = \frac{1}{4\Lambda g_A^2} F_{\mu\nu} F^{\mu\nu} \quad (27)$$

with

$$g_A^2 \propto m \quad (28)$$

where $m = |\langle \pi \rangle|$ is the fermion mass. The pion action will be a sigma model. If we change the normalization on the pion field so that $|\pi| = 1$, we get the model

$$L_M = \frac{1}{2g^2} (\partial_\mu \pi^a)^2 + \frac{(m_\pi^\perp)^2}{2g^2} \pi^1 \pi^2 \pi^3 \quad (29)$$

where the coupling constant g^2 is proportional to m^{-1} and the mass m_π^\perp represents the breaking of continuous symmetry by lattice effects.

We have chosen the mass term for the pion to cause the pion to prefer to condense in a way that gives rise to a mass M_{12} . In the projected mean-field calculation above, we considered states invariant under the rotational symmetry, so that $|m_1| = |m_2| = |m_3|$. This provided two inequivalent perturbations. In one, we increased $|t_{ij}|$ on hexagons and triangles; in the other we increased $|t_{ij}|$ on a loop of length twelve. While at the mean-field level symmetry breaking does not occur, from the projected mean-field calculation we can still argue that the preferred symmetry breaking pattern would be given by a mass matrix M_{12} . Other patterns are of course possible, and comparison with numerics provides some evidence that a staggered mass is also a possibility, at least for small systems; in the conclusion we discuss possibilities of numerically testing the preferred mass pattern.

In the continuum field theory, the pion mass $(m_\pi^2)^{ab}$ is ultraviolet divergent. However, lattice symmetry forces the masses of the pion modes to be the same before condensation. In order to use the continuum theory to estimate m_π^\perp after condensation, we need to turn to the cubic interaction terms in π . These are

$$\int d^3x g_3 \pi_1 \pi_2 \pi_3 \quad (30)$$

with a cubic coupling constant g_3 that is generically of order unity. Inserting an expectation value of π of order m , we obtain a quadratic term in π . Including this quadratic term in $(m_\pi^2)^{ab}$, this will cause the masses of the different pion modes to differ by order m so that m_π^\perp will be of order m .

However, we can obtain a better estimate of the mass difference numerically from the the projected mean-field calculation of energy; while we did not obtain pion condensation at the mean-field level, for a given expectation value of the pion field, we can use the *difference* in mean-field energies for various continuous rotations of the pion field to obtain an estimate of the pion gap. Using the numerical estimate for the triplet gap, and hence the estimate for the fermionic mass m , we have calculated the projected mean-field energies for taking $M = mM_{12}$ and $M = mM_6$. The difference in energies is $0.000396J$ per 12-site cell, so that $m_\pi^\perp \approx \sqrt{0.000396mJ}$. This is small enough that we can ignore this mass for most purposes. Evidently, the cubic coupling constant g_3 is very small.

While the pion is already gapped by lattice effects, instantons will gap the gauge field, leading to confinement of the spinons. The gauge field describes compact QED in 2+1 dimensions, which is confining for all g_A [28]. The gauge coupling is proportional to m , so that the action for an instanton will be of order

$$S \propto \frac{\Lambda_0}{m} \quad (31)$$

The instanton density is proportional to e^{-S} . In the weak coupling limit, the instantons lead to a gap for the gauge field of order $\Lambda_0 e^{-S}$. As this is exponentially small, we can ignore the gap in the gauge field.

VIII. FINITE SIZE SYSTEMS AND CHERN NUMBERS

In this section we will consider some effects of finite size systems to begin comparison with numerics. First we will consider some complications in defining the parent state on systems with an odd number of sites, which force the system to have some net flux. Then we will show how this leads to a degeneracy in the spectrum and nonvanishing Chern numbers for the states under twist in the spin boundary conditions. Finally, we will discuss some effects of finite size for even size systems.

One of the most interesting results found in numerical studies of odd size systems is a non-vanishing Chern number [20] for the ground state of ± 1 . This is a quantity that provides an analogue for a spin system of the quantum Hall effect [29]. Since the Hamiltonian of equation (1) does not explicitly break time-reversal symmetry, a non-vanishing Chern number requires a spontaneous breaking of time-reversal symmetry. However, the spontaneous breaking of time-reversal symmetry is not enough, as other spin systems that break this symmetry have vanishing Chern number [29]; the kagomé antiferromagnet may be the first Hamiltonian with time-reversal and parity symmetry where a non-vanishing Chern number has been observed. In order to understand the appearance of the Chern number, we must first understand how to form the parent state on an odd size system.

The systems studied numerically have periodic boundary conditions, so that they live on a torus. On system defined on a torus the net flux penetrating the surface must be an integer multiple of 2π . One can also add solenoid fluxes, θ_1, θ_2 , defining the phase that the spinon acquires when traversing a topologically nontrivial closed loop around the torus. For simplicity, we will use coordinates on the torus which range from 0 to 2π in both directions, although in actuality for the kagomé lattice the systems considered are not square.

The parent state has π flux through each hexagon. On a system with N sites, there are $N/3$ hexagons, and so on a system with an odd N , one would like to have a net flux through the system that is an odd multiple of π . This is not possible, and so the system must have some additional flux so that the total is a multiple of 2π . For example, on a system with $N = 27$, there are 9 hexagons, so the system can put $\pi \pm \frac{\pi}{9}$ flux through each so that the total flux is either 8π or 10π . The system then must become chiral and break time reversal symmetry since it cannot construct the parent state.

A qualitative way of describing this effect is to say that for a system with an odd number of sites, there is an unpaired spinon, which has a chirality. The spinon then couples to the gauge field and produces a flux.

Given this net flux through the system, let us consider the effective Dirac equation for the spinons. The results we get for the Chern number do not rely on the Dirac description, and can be derived directly from the lattice model; we feel that the Dirac method is more elegant and gives more physical insight.

The Dirac particles feel the extra flux that has been added, and so the spinons move in a magnetic field, such that the net flux the spinons feel is exactly $\pm\pi$. Again, there seems to be a contradiction, since it is not possible for the system to have a net flux of $\pm\pi$ flux through the torus. The answer to the contradiction is that the Dirac particles have an extra chirality index. So, in addition to including solenoid fluxes for the Dirac equation, the Dirac particles can change chirality when completing a loop around the system. Let us then generalize the solenoid flux to a pair of 4-by-4 matrices U_1, U_2 , describing the change in the wavefunction when the particle completes a loop.

Then, when the particle traverses a loop around the torus from $(0, 0)$ to $(0, 2\pi)$ to $(2\pi, 2\pi)$ to $(2\pi, 0)$ to $(0, 0)$, the wavefunction gets multiplied by

$$- U_1 U_2 U_1^\dagger U_2^\dagger \quad (32)$$

where the minus sign is from the magnetic flux through the torus. Since equation (32) must be equal to 1, we find that U_1, U_2 necessarily anti-commute.

One may regard the matrices U_1, U_2 as arising from a non-Abelian gauge field connecting opposite chiralities of the spinons. The commutator of the matrices represents an additional flux of π from the non-Abelian field, giving a total flux of 2π on the torus. The extra π flux from the non-Abelian field is the flux that arises from having an odd number of hexagons on the lattice, so that when the particle completes the given loop around the lattice it has enclosed an odd number of π fluxes. One sees that the non-Abelian flux is localized at a point, although one must be careful that this localization at a point does not imply a breaking of translational symmetry.

The addition of matrices U_1, U_2 is natural from the lattice point of view. The unit cell which includes both chiralities of Dirac particles is 12 sites, while the smallest unit cell possible for the parent state is 6 sites. Since there is no way to cover an odd size lattice with 6 or 12 site unit cells, something must scatter between chiralities, as when the particle completes a loop it has changed between chiralities.

To give a very simple example of this, consider a one-dimensional ring with an odd number of sites. The natural unit cell for the a one-dimensional chain is two-sites, to include both Dirac points. If the particle moves around an odd-length ring, two sites at a time, it must return to the starting point displaced by half a unit cell.

To give a slightly more complicated example, consider the π -flux phase of the square lattice [30] for a system of 9 sites, shown in figure 5. Solid lines represent bonds within the cell of 9 sites, while dotted lines represent bonds to provide toroidal boundary conditions. There are 9 squares in the system, and so there will be $\pi \pm \frac{\pi}{9}$ flux through each square. 4 of the squares lie within the cell and are labeled 1-4, another 4 lie to the sides and are labeled 5-8, while the 9th square lies in the corner. The natural unit cell for the Dirac particles is 4 sites, so when a particle completes a loop around the torus it is displaced by half a unit cell. The wavefunction is multiplied by a matrix U_1 for a loop in the \hat{x} -direction and a matrix U_2 for a loop in the \hat{y} -direction. Precisely due to the odd number of squares, one finds that the matrices U_1, U_2 anti-commute. It is natural to think of the non-Abelian flux as arising from the π -flux through the 9th square, on the corners.

Returning to the kagomé lattice, let us now look at the wavefunctions of the Dirac equation with this magnetic flux. It is convenient to find the wavefunctions by enlarging the torus by a factor of two in each direction, as shown in figure 5. The + and - symbols in the figure denote the chirality of the particle in each quadrant. When the particle completes a circuit on the original torus, it changes chirality, and hence moves into a different quadrant of the enlarged torus, while picking up a phase.

The net flux on the enlarged torus is equal to 4 times the flux on the original torus, or 4π . One might imagine that there will be extra sources of π -flux on the enlarged torus at the points where the quadrants meet. However, since the π non-Abelian flux is purely a result of an odd number of hexagons on the original torus, we can drop the extra sources of flux on the enlarged torus, and we are left with an explicitly translationally invariant problem of a Dirac particle moving in a constant magnetic field.

On the enlarged torus, the Dirac equation becomes a two-component equation

$$\left(iE\sigma_z + \sigma_x(A_x + i\partial_x) + \sigma_y(A_y + i\partial_y) \right) \psi = 0 \quad (33)$$

Taking the square we find

$$E^2\psi = \left((i\partial_x - A_x)^2 + (i\partial_y - A_y)^2 + \sigma_z B \right) \psi \quad (34)$$

This is the well known equation for a Dirac particle in a magnetic field, and has Landau levels.

Since the net flux through the enlarged torus is equal to 4π , there are two-states in each Landau level for each σ_z , hence four states for each Landau level in total. As we are dealing with a two component equation, only one sign of E is allowed in equation (34) for given σ_z .

Therefore, the energy levels on the enlarged torus are doubly degenerate. However, the enlarged torus has an unphysical degree of freedom: opposite quadrants describe the state of the particle on the original torus. So, the energy levels on the original torus are only singly degenerate and the spectrum is discrete with one level at zero energy. This is the relativistic generalization of Landau levels. For an odd size system, all Landau levels below the zero energy are occupied, and hence filled, for both spin up and spin down particles, while the zero energy level is occupied only by one unpaired spinon.

Numerically, the ground state of the many-body system has been seen to have an extra degeneracy factor of two, beyond the trivial spin degeneracy. This is a consequence of the spontaneous generation of the magnetic field, so that the system can pick either sign for the field.

An interesting way of viewing the Landau levels is that we have π Abelian flux, implying that there are 1/2 states per Landau level. Multiplying the 1/2 by a factor of two for chirality degeneracy, we get one state per Landau level.

We can now introduce the Chern number of the system, which characterizes a transverse response of spin currents. Let us adjust the boundary conditions of the system so that

$$S^\pm(x, y) = e^{\pm i\phi_1} S^\pm(x + 2\pi, y) \quad (35)$$

$$S^\pm(x, y) = e^{\pm i\phi_2} S^\pm(x, y + 2\pi) \quad (36)$$

where ϕ_1, ϕ_2 are angles.

If the ground state is a wavefunction Ψ , then the Chern number is defined as the integral

$$\frac{1}{2\pi} \int \int \langle \frac{\partial \Psi}{\partial \phi_1} | \frac{\partial \Psi}{\partial \phi_2} \rangle d\phi_1 d\phi_2 \quad (37)$$

This number is quantized, and non-vanishing only for complex states. Since the Hamiltonian does not break time-reversal symmetry, complex conjugate states are degenerate with opposite Chern numbers.

In the presence of these boundary conditions, the spinon boundary conditions, with additional self-generated fluxes θ_1, θ_2 , become

$$\psi_u^\dagger(x, y) = e^{i\frac{\rho_u^\dagger}{2}} \psi_u^\dagger(x + 2\pi, y) \quad (38)$$

$$\psi_d^\dagger(x, y) = e^{i\frac{\rho_d^\dagger}{2}} \psi_d^\dagger(x + 2\pi, y) \quad (39)$$

where

$$\rho^{u,d} = (2\theta_1 \pm \phi_1) \quad (40)$$

and similarly for the other direction. The 2π periodicity in ϕ is not obvious from equation (38,39), but the ability of the system to adjust θ produces the desired periodicity.

To give a simple example of how a system can adjust θ , consider a system of 4 sites on a ring. In the absence of a twist in boundary conditions ϕ , the system places $\theta = \pi$ flux through the ring. As ϕ increases, θ remains equal to π , and the mean-field energy of the system gradually increases until $\phi = \pi$. At this point, θ jumps to 0, and the mean-field energy begins to decrease for increasing ϕ . So, as ϕ varies from 0 to 2π and θ jumps as described above, we find that $\frac{\rho}{2} = \frac{(2\theta + \phi)}{2}$ varies from π to $\frac{3\pi}{2}$ to $\frac{\pi}{2}$ to π . In order for θ to jump like this, the spinon states with $\frac{\rho}{2} = \pi \pm \frac{\pi}{2}$ must be degenerate.

Now, we can look at the Chern number of the system, assuming non-interacting spinons. It then amounts to a Chern number calculation of the fermionic wavefunctions. Assuming non-interacting spinons, we can get the change in Ψ in equation (37) from the change in the spinon wavefunctions.

While in general the wavefunction gets multiplied by a matrix on moving around the original torus, only the $U(1)$ part of this matrix adjusts in response to changes in ϕ . The $U(1)$ part of the matrix is just the angle θ . Carrying out the calculation on the enlarged torus, we find that the boundary conditions become

$$\psi_u^\dagger(x, y) = e^{i\rho_u^\dagger} \psi_u^\dagger(x + 4\pi, y) \quad (41)$$

and similarly for down spinons.

So, we wish to compute

$$\frac{1}{2\pi} \int \int \langle \frac{\partial \psi}{\partial \rho_1^{u,d}} | \frac{\partial \psi}{\partial \rho_2^{u,d}} \rangle \frac{\partial \rho_1^{u,d}}{\partial \phi_1} \frac{\partial \rho_2^{u,d}}{\partial \phi_2} d\phi_1 d\phi_2 \quad (42)$$

summed over all spinon wavefunctions ψ .

In equation (41) the periodicity in ϕ seems obvious even without θ , as on the enlarged torus the periodicity of the spinon wavefunctions in response to a twist in boundary conditions is halved in both directions. However, we have introduced the degeneracy of two on the enlarged torus representing the fact that on the original torus the wavefunctions are periodic in (ρ_1, ρ_2) with periods $(0, 2\pi)$ and (π, π) but not with period $(0, \pi)$, and as a result only half the possible wavefunctions on the enlarged torus are physical.

In order to keep the wavefunction in the physical sector, θ must jump discontinuously by π as ϕ changes, and as a result for a given spinon state we only integrate equation (42) over half the torus of possible phases (ρ_1, ρ_2) .

The fact of integrating over half the torus, or equivalently the fact that the Landau levels contain one physical and one unphysical wavefunction, does not prevent a defining of the Chern number for the spinon wavefunctions. When θ jumps it connects two degenerate states, and so the contribution of equation (42) to equation (37) must still be quantized as an integer which we can still refer to as a Chern number for the spinon.

Within the lattice formulation there are no further conceptual problems and we must simply compute the integrals, but within the continuum Dirac equation we must account for the negative energy sea. The correct understanding of this was found by Haldane [31].

One must add a massive regulator field, and compare the difference in Chern number between the massless and massive fields. The massive field has the same Landau level spectrum, but no zero mode. So, the difference in Chern numbers is due to the zero mode, which sits in the lowest Landau level. There are two states in the lowest Landau level, one physical and one unphysical. It is the physical state that carries the Chern number of ± 1 , giving the ground state of the spin system a net Chern number of ± 1 , as seen numerically [20].

We expect that the low-lying states will continue to have an odd Chern number, in agreement with numerical results. If a particle-hole pair is excited within the Dirac band near the Dirac point, the Chern number will not change. If the particle is excited from the band edge, the Chern number can change by ± 2 . Only if a particle is excited from the flat band to the Dirac band can the Chern number change by ± 1 , giving rise to an even Chern number. However, these states will be much higher in energy. One can also consider excited states with net Abelian flux be equal to $3\pi, 5\pi, \dots$

It is very interesting to think about these possible excited states which may have more than π flux for the Dirac particles. The two-component particles carry a σ_z index, which will couple to the magnetic field. If a large field is induced, a number of spinons of the same σ_z will be produced in the zero mode, so that the total number of spinons in the zero mode is odd. For one spinon we had one filled Landau level, with one particle. With several spinons one might be able to construct fractional Hall states of spinons.

We have argued that in the thermodynamic limit the system will acquire a mass. On an odd size lattice, the mass term must change sign somewhere, as the lattice cannot be tiled with 12-site unit cells. At the domain wall where the mass changes sign, one expects to trap a midgap state, so there still should be a zero mode, even with mass. This may permit the nonvanishing Chern number to survive.

Returning to even system size, let us consider the size dependence of the triplet gap. The energy of the spinon is $E = \sqrt{(v_f k)^2 + m^2}$. In the absence of a solenoid flux, the smallest k would be equal to zero, but by creating a solenoid flux the energy can be improved and the smallest k will be of order the inverse linear dimension of the system, or $N^{-1/2}$. As a result, the triplet gap is decreasing with system size, in agreement with numerics. By twisting the spin boundary conditions one may be able to reduce the gap to $S_z = \pm 1$ excitations. It would be interesting to look for this effect.

Further, in the presence of these solenoid fluxes, other fermionic states with $k \neq 0$ will become approximately degenerate with the $k = 0$ fermionic state. This means that a spatially varying mass term which scatters between k states can open a gap just as well as the spatially constant mass term can. This will be important when we consider the low energy Goldstone excitations on finite size systems, below.

IX. GOLDSTONE MODES, TOWER STATES, AND NUMERICS

After breaking a symmetry, and giving mass to the fermions, the system is left with low energy pion and gauge modes. Above, we argued that the gap for these modes is too small to be seen in numerical calculations. In this section, we will treat these modes as gapless and discuss the energy spectrum that results for finite size systems to compare with numerical calculations.

It is known [32] that breaking a continuous symmetry gives rise to two kinds of low energy modes. First, there are the Goldstone modes with non-zero wavevector k . In the case of our pion and gauge modes, the energy is then proportional to k . For a $2 + 1$ dimensional system with N sites, the lowest k is proportional to $N^{-1/2}$ and so the lowest Goldstone excitation has energy proportional to $N^{-1/2}$.

Second, there is the “tower” of $k = 0$ modes. These correspond to global rotations of the entire system, and have an energy proportional to N^{-1} .

Numerical diagonalization [33] of the *triangular* lattice Heisenberg anti-ferromagnet, which has Néel order, shows very clearly the distinction between the tower of states, and the $k \neq 0$ states (spin waves). However, no such distinction is found in the kagomé lattice, no separation between low energy modes of energy N^{-1} and $N^{-1/2}$. Within our model, this is to be expected for $N = 36$. Since the effective action of the pion and gauge fields arises from integrating out the fermions, this action must be approximately relativistic, with the same velocity as the fermions. So, even without explicit calculation, we can obtain the energy of the lowest $k \neq 0$ mode directly from the velocity appearing in Dirac

equation. For the largest numerical diagonalizations, systems with $N = 36$ total sites or 3 of our 12-site unit cells, this energy turns out to be of order the triplet gap, and so this Goldstone mode is too high in energy to appear in the continuum of low energy singlets.

The only states that will be observed in numerics are states in the tower. We can obtain the energy of these states from equation (29), assuming that $\pi(x)$ is constant. Then we get, assuming small m_π^\perp ,

$$L = \frac{N\Lambda_0^{-2}}{g^2}(\partial_t\pi^a)^2 \quad (43)$$

where $N\Lambda_0^{-2}$ is the area of the system. The states of this will be spherical harmonics, perturbed by mass term. With $g^2 \propto m^{-1}$, these states will have an energy proportional to

$$\frac{\Lambda_0^2}{Nm} \quad (44)$$

and so for sufficiently large N will be below the triplet gap. A more precise knowledge of the prefactors will be needed to determine whether this is low enough to correspond to the low energy modes seen numerically.

There will also be “tower” states for the gauge field, which correspond to different solenoid fluxes through the system. The energy for these can be obtained from equation (27) assuming that A_μ is constant over the sample. To get the energy for these we have to remember that the gauge group is compact, and realize that $F^{\mu\nu}$ is derived from a set of $U(1)$ matrices with a lattice length Λ_0 . Then, the energy of the gauge states is proportional to

$$\frac{m}{N} \quad (45)$$

which is definitely below the triplet gap and certainly small enough to be the origin of some of the low energy modes in numerics.

There is one puzzle involved in the tower states. It was observed numerically that, on 36 site samples, the energy of the lowest energy state of the system at given total momentum did not vary appreciably across the Brillouin zone [20]. This may seem to be in contradiction to the hypothesis that the low energy states come from the tower. The resolution of this may lie in realizing that there are only 4 inequivalent points in the Brillouin zone of the system. One of these is at $k = 0$, while including a constant nonvanishing mass term M_{12} also breaks translational symmetry on the kagomé lattice, and can give one more point in the Brillouin zone. To obtain the last points in the Brillouin zone, one must remember that for small systems there can be other symmetry breaking patterns with staggered mass, breaking translational symmetry in different ways, as discussed in the section on finite size effects.

This would imply that for sufficiently large system sizes one would find a more significant variation in the energies across the Brillouin zone, as only some of the states could be obtained from the tower. One would also find for 36 site systems that the spinon solenoid fluxes would change under a twist in spin boundary conditions, and so the fermionic states at different k would lose their degeneracy, leading to a change in energy of some of the $k \neq 0$ states when varying boundary conditions.

Another possibility is that, even for infinite systems, short-distance effects lead to the production of a staggered-mass pattern, in the style of the “perfect hexagon” state [12] discussed above. The staggered mass pattern gives rises to an enlarged unit cell, and makes it possible to get low energy states at the other points in the Brillouin zone.

X. FURTHER COMPARISON WITH NUMERICS

In addition to the existence of the low energy states, we make further comparison with numerics for the many-body density of states and the dimer-dimer correlation functions.

Assuming the existence of a low-energy bosonic mode with linear dispersion relation, so that the single-particle density of states scales linearly with energy, one would expect the many-body density of states at energy E to scale for large systems as an exponential of $E^{2/3}$. The quadratic behavior of experimentally measured specific heat is in agreement with this.

Since we have argued that the low-energy states in numerical calculations are largely “tower” states, it is impossible to extract the density of states in a large system from the finite size density of states. The true exponential growth can only be seen when the $k \neq 0$ modes become important.

In this regard, the numerically measured [20] *quadratic many-body density of states* at very low energies does not say anything about the dispersion of the Goldstone modes. Instead, it is a reflection of the fact that if a finite number of “tower” modes are excited then the many-body density of states is a power law.

For the dimer-dimer calculations we can make a more direct comparison with a numerical calculation of these correlations on a 36 site system [6]. In the thermodynamic limit, the dimer-dimer correlation function should be long-ranged, reflecting the existence of a non-zero m_{12} .

However, there is also a short-range fermionic contribution to the dimer-dimer correlation functions, and for 36 site systems, so that the system size is smaller than the correlation area of the fermions, we can ignore the effect of a non-zero m_{12} on the dimer-dimer correlation function and directly study the correlation functions of massless fermions.

If we are interested in a dimer-dimer correlation function

$$C_{(i,j)(k,l)} = \langle (\vec{S}_i \cdot \vec{S}_j)(\vec{S}_k \cdot \vec{S}_l) \rangle - \langle (\vec{S}_i \cdot \vec{S}_j) \rangle \langle (\vec{S}_k \cdot \vec{S}_l) \rangle \quad (46)$$

we can express this, under the assumption of weak spinon interaction, directly in terms of the spinon Green's functions. Writing each spin operator in terms of spinons and considering various contractions we obtain

$$C_{(i,j)(k,l)} = -4\text{Re}(G_{ij}G_{jk}G_{kl}G_{li}) - 4\text{Re}(G_{ij}G_{jl}G_{lk}G_{ki}) - \text{Re}(G_{ik}G_{kj}G_{jl}G_{li}) + \frac{1}{2}|G_{ik}|^2|G_{jl}|^2 + \frac{1}{2}|G_{ij}|^2|G_{kl}|^2 \quad (47)$$

To obtain quantitatively accurate answers, we must include the effects of projection within an approximation like that used above, projecting on site i, j, k, l , requiring that there be one fermion on each of these four sites. We have done this at 3 different levels of approximation.

At the lowest level, we have noted that the wavefunction before projection will have one fermion on each of these sites is roughly the product of the probability that it will have one fermion on each of i, j by the probability that it will have one fermion on each of k, l . Given that $|G_{ij}| = 0.221383\dots$ for neighboring i, j , we should replace equation (47) by

$$C_{(i,j)(k,l)} = \kappa \left(-4\text{Re}(G_{ij}G_{jk}G_{kl}G_{li}) - 4\text{Re}(G_{ij}G_{jl}G_{lk}G_{ki}) - \text{Re}(G_{ik}G_{kj}G_{jl}G_{li}) + \frac{1}{2}|G_{ik}|^2|G_{jl}|^2 + \frac{1}{2}|G_{ij}|^2|G_{kl}|^2 \right) \quad (48)$$

where

$$\kappa = (1.9264)^2 \quad (49)$$

is the desired factor of $(\frac{4}{1+16|G|^4})^2$.

At a more refined level, we have carried out the computation projecting on all four sites exactly. At the third level of approximation we have started to project out onto additional sites as well. We have calculated the correlation functions in this approximation, in the limit of an infinite system size, for pairs of bonds that can both be written in the same 12-site unit cell. We compare the result to results from numerics on a 36-site system [6]. We do not consider pairs of bonds that cannot be written in the same unit cell, as at this separation, finite-size effects will become important in the numerics and the comparison will become impossible. We could in principle improve on our comparison with numerics by computing the spinon correlation functions in a 36-site system also, in which case it should be possible to compare all bonds, but we have not done this.

The results are shown in table I, where in the column Theory I we show the simplest approximation, and in the column Theory II we show the second level of approximation. Qualitatively, the theory works quite well on the signs even at this level, getting 9 out of 12 correct. The only signs that the theory gets wrong at this level occur when the theory predicts a very small value ($< .01$) for the correlation function.

To improve this result, we included the third level of approximation in which we also project out onto a fifth site (m) for those dimer correlation functions such that there is one and only one site (m) which neighbors both dimers. In the column Theory III we show this level of approximation, as well as the particular site (m) that we picked. Once this is done all the signs work out for 11 out of 12 correlations, and the qualitative agreement is almost perfect.

The magnitudes work out less well, as most of the dimer-dimer correlations are far too small within the spinon calculation. However, RVB calculations are quite poor at getting long range correlations without including some gauge fluctuations. For example, in the one-dimensional Heisenberg antiferromagnet, the spins on the same sublattice are uncorrelated [34]. By including gauge fluctuations, this result can be substantially improved [35].

For the largest positive correlation function, $C_{(6,7)(1,8)}$, the magnitude does work out well even at the simplest approximation. However, for the largest negative function, $C_{(6,7)(11,5)}$, the magnitude is off by roughly a factor of 5, until we go to the third level of approximation, at which point the magnitude becomes roughly correct. We can hope that a better inclusion of fluctuations will improve these results, just as it has done for the one-dimensional chain. Perhaps projecting on an entire 12-site cell would give better results, as suggested by the improvement in the results in column III. Detailed calculations of projection for some trial wavefunctions on the kagomé lattice have been performed by Hsu and Schofield [14]. A similarly detailed calculation for our parent state would be of interest.

XI. CONCLUSION

In conclusion, we have constructed an RVB state on the kagomé lattice, the “parent state”, which has a Dirac structure. Consideration of the various mass perturbations to the Dirac equation unifies several other previously suggested long-range states of the kagomé lattice Heisenberg antiferromagnet, with the exception of the BCS [14] state and the bosonic $Sp(2N)$ state [13].

While at the projected mean-field level the chiral spin liquid appears to be the best RVB state, we have argued by a renormalization group treatment that fluctuations provide a mechanism for stabilizing a state with a nonchiral mass term. The numerical evidence also argues against a chiral state. We have then proceeded to explicit comparison with numerics, taking as input only one quantity, the triplet mass gap.

The physical idea behind our construction is that, given massless fermions, the system must ultimately try to break some symmetry to give mass to the fermions. There are many ways of doing this, but they all correspond to either introducing chirality, or to introducing some kind of spin-solid state in which the system dimerizes the t_{ij} . If we ignore the chiral state, we must have some kind of spin solid: we have proposed one possible spin solid and its attendant pseudo-Goldstone excitations. Other spin solids are possible, and may in fact be realized in favor of our proposal, but the general principle that the massless fermions must break a symmetry and produce pseudo-Goldstone excitations should be robust. Two other possibilities for spin solids that must be considered are the constant M_6 solid, and the perfect hexagon system with spatially varying M_6 .

Experimentally, it may be possible in principle to detect the spin-Peierls order. Although this as appears as long-range order only in 4 spin correlation functions, it should give rise to a short-range oscillatory piece in the spin-spin correlation function. Since the spin-spin correlation function decays exponentially and the dimerization is weak, this would be very difficult to detect, but in principle it is possible via neutron scattering.

Theoretically, more work is needed on the fluctuations about the parent state. Doing a Gutzwiller projection of the wavefunctions on a 36-site lattice should enable much more direct comparison with numerics, especially for the dimer-dimer correlation functions.

Numerically, it may be possible to confirm the identification of the low-energy states with tower states from symmetry breaking. If one computes a dimer-dimer correlation function with the same pair of sites taken at two different times it may be possible to see the oscillations in the mass field. This may be difficult, though, given the relatively weak amount of dimerization present and the problem of extracting the contribution of the mass term to dimer-dimer correlation functions from the background of the fermionic contribution. Similarly, one can try to compute a susceptibility to spin-Peierls ordering by explicitly dimerizing coupling constants J in equation (1). If indeed the system wishes to spontaneously order in the thermodynamic limit, then the susceptibility to dimerization should be large. This may make it possible to unambiguously determine whether the system prefers the M_{12} or other ordering pattern.

It might also be interesting numerically to look at model systems in which the Hamiltonian has additional terms coupling to the chirality operator on each triangle. This might make it possible to probe the stability of the system to the chiral mass term, as well as providing some interesting states in which the Dirac fermions are moving in a large net magnetic field.

XII. APPENDIX: AN INTERESTING FLAT BAND CASE

When the system has flux $\pi/4$ through each triangle and flux $\pi/2$ through each hexagon the band structure becomes very peculiar. Using a 12-site unit cell, we find that the lowest band is doubly degenerate, and almost exactly flat. The next band above that is quadruply degenerate and exactly flat. The higher bands, which are all empty, are not flat.

It is very unlikely that any such state could be stabilized. We have argued above the the kagomé lattice is not a chiral spin liquid. However, it may be possible to add chirality operators to the Hamiltonian to tune the flux through the triangles.

In this case, the physics of the flat band state would be very amusing. We are used to the fact that in, for example, the one-dimensional Heisenberg antiferromagnet, one can deduce that the spin-1 excitations are composite objects of two spinons by looking at the excitation spectrum. Since the energy of the spin-1 object is a sum of two different energies, there is a continuum of possible energies. When, however, one of the two spinons is a hole excitation from a flat band, the energy is constant over the band, and there is no sign of the composite nature of the spin waves when looking at their energy spectrum. One would have a situation with one spinon hopping freely over the lattice, while the other spinon sits unmoving on a given unit cell!

XIII. ACKNOWLEDGEMENTS

I would like to thank S. Sondhi for suggesting the problem of the kagomé antiferromagnet, and for many useful discussions and insights. I would also like to thank R. Moessner for useful discussions on theory and experiment in frustrated antiferromagnets, V. N. Muthukumar for discussions on RVB ideas, A. Vishwanath for discussions on Chern numbers, and S. Sachdev for clarifying the estimate of the pion gap.

- [1] C. Zeng and V. Elser, Phys. Rev. B **42**, 8436 (1990).
- [2] E. Manousakis. Rev. Mod. Phys. **63**, 1 (1991) and references therein.
- [3] D. A. Huse and V. Elser, Phys. Rev. Lett **60**, 2531 (1988).
- [4] T. Jolicoeur and J. C. Le Guillou, Phys. Rev. B **40**, 2727 (1989).
- [5] L. Capriotti et. al., Phys. Rev. Lett. **82**, 3899 (1999).
- [6] P. W. Leung and V. Elser, Phys. Rev. B **47**, 5459 (1993).
- [7] M. G. Townsend, G. Longworth, E. Roudaut, Phys. Rev. B **33** 4919 (1986).
- [8] S. H. Lee et. al., cond-mat/9705014.
- [9] A. S. Wills. et. al., cond-mat/9607106.
- [10] X. Obradors et. al., Sol. St. Comm. **65**, 189 (1988).
- [11] A. P. Ramirez, “Geometrical Frustration”, to appear in Handbook of Magnetism.
- [12] J. B. Marston and C. Zeng, J. Appl. Phys. **69**, 5962 (1991).
- [13] S. Sachdev, Phys. Rev. B **45**, 12377 (1992).
- [14] T. C. Hsu and A. J. Schofield, J. Phys.-Cond. Matt. **3**:(41), 8067 (1991).
- [15] F. Mambrini and F. Mila, preprint cond-mat/0003080.
- [16] V. Elser, Phys. Rev. Lett. **62**, 2405 (1989).
- [17] F. Mila, Phys. Rev. Lett. **81**, 2356 (1998).
- [18] G. Baskaran, Z. Zou, and P. W. Anderson, Solid State Commun. **63**, 973 (1987).
- [19] P. W. Anderson, Science **235**, 1196 (1987).
- [20] Ch. Waldtmann et. al, preprint cond-mat/9802168.
- [21] D. S. Rokhsar, Phys. Rev. B **42**, 2526 (1990).
- [22] V. Kalmeyer and R. B. Laughlin, Phys. Rev. Lett. **59**, 2095 (1987).
- [23] S. Sachdev and M. Vojta, cond-mat/9910231.
- [24] T. C. Hsu, Phys. Rev. B **41**, 11379 (1990).
- [25] V. N. Muthukumar, private communication.
- [26] D. S. Rokhsar, Phys. Rev. Lett. **65**, 1506 (1990).
- [27] J. B. Marston and I. Affleck, Phys. Rev. B **39** 11538 (1989).
- [28] A. M. Polyakov, Gauge Fields and Strings (Harwood Academic Publishers, New York, 1987).
- [29] F. D. M. Haldane and D. P. Arovas, Phys. Rev. B **52**, 4223(1995).
- [30] On the square lattice the system does not need to form the π -flux states. It can also form a d-wave superconducting state, which is not equivalent to the π -flux for odd size lattices. The d-wave state will not give rise to a Chern number. However, the π -flux state on the square lattice is still a nice example to consider.
- [31] F. D. M. Haldane, Phys. Rev. Lett. **61**, 2015 (1985).
- [32] P. W. Anderson, Phys. Rev. **86**, 694 (1952).
- [33] P. Lecheminant et. al., Phys. Rev. B **56**, 2521 (1997).
- [34] D. P. Arovas and A. Auerbach, Phys. Rev. B **38**, 316 (1988).
- [35] D. H. Kim and P. A. Lee, Annals. Phys. **272**, 130 (1999).

TABLE I. Comparison of $C_{(i,j)(k,l)}$ between numerical and spinon calculations. See figure 1 for labeling of points in unit cell. See text for discussion of various approximations.

| (i,j)(k,l) | Numerics | Theory I | Theory II | Theory III | (<i>m</i>) |
|-------------|----------|-----------|------------|------------|--------------|
| (6,7)(1,8) | 0.04337 | 0.08242 | 0.06249 | | |
| (6,7)(8,2) | -0.01416 | -0.01107 | -0.001318 | -0.01686 | (1) |
| (6,7)(9,3) | -0.00646 | -0.001041 | -0.0004279 | -0.022153 | (8) |
| (6,7)(10,3) | 0.01178 | 0.001043 | 0.0005004 | | |
| (6,7)(10,4) | -0.01045 | -0.001040 | -0.0005008 | | |

| | | | | | |
|--------------|----------|------------|------------|-----------|------|
| (6,7)(11,5) | -0.06510 | -0.02499 | -0.0112132 | -0.083829 | (12) |
| (11,10)(7,8) | 0.01221 | 0.018885 | 0.00938 | | |
| (11,10)(9,8) | -0.00113 | -0.01824 | -0.0025 | -0.01395 | (3) |
| (11,10)(2,9) | 0.00108 | 0.0001619 | 0.00559 | -0.007171 | (3) |
| (6,7)(11,4) | 0.01322 | -0.0009778 | -0.000327 | 0.001416 | (12) |
| (11,10)(2,8) | 0.00045 | -0.004377 | -0.001964 | 0.00386 | (9) |
| (6,7)(9,2) | 0.01322 | -0.0009788 | -0.000328 | 0.001415 | (8) |

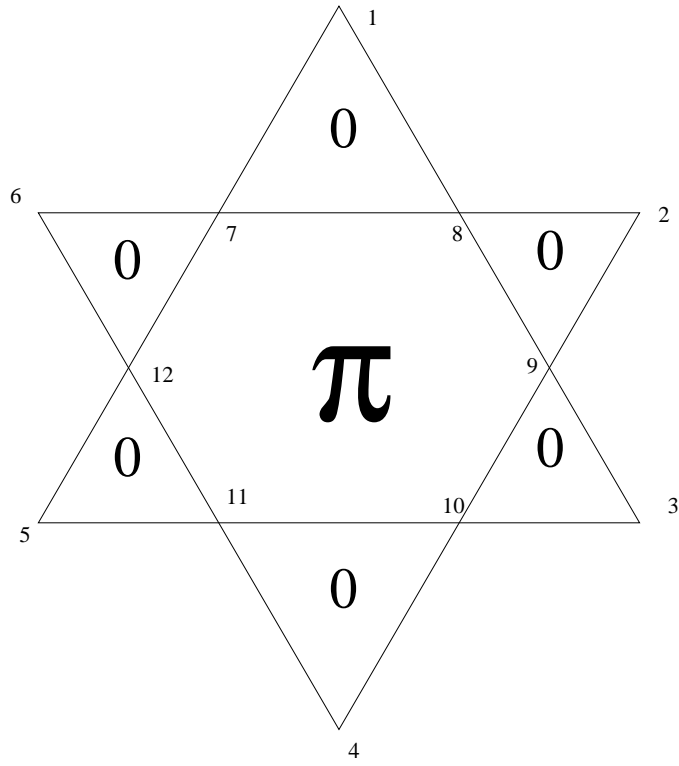


FIG. 1. 12-site unit cell, with fluxes indicated. Small numbers are used to label points for reference.

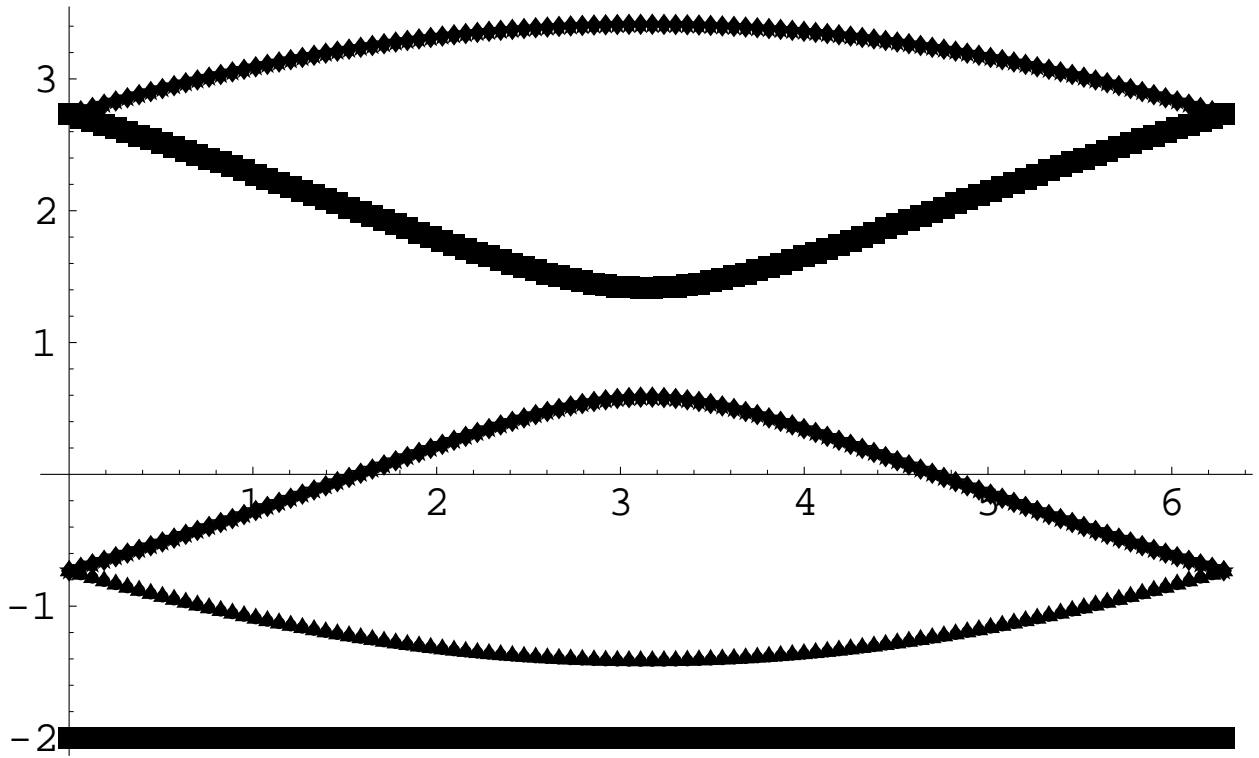


FIG. 2. Band structure for the parent state. We scan along varying momenta in the \hat{x} direction, at vanishing momentum in the $\frac{\hat{x}}{2} + \frac{\sqrt{3}\hat{y}}{2}$ direction.

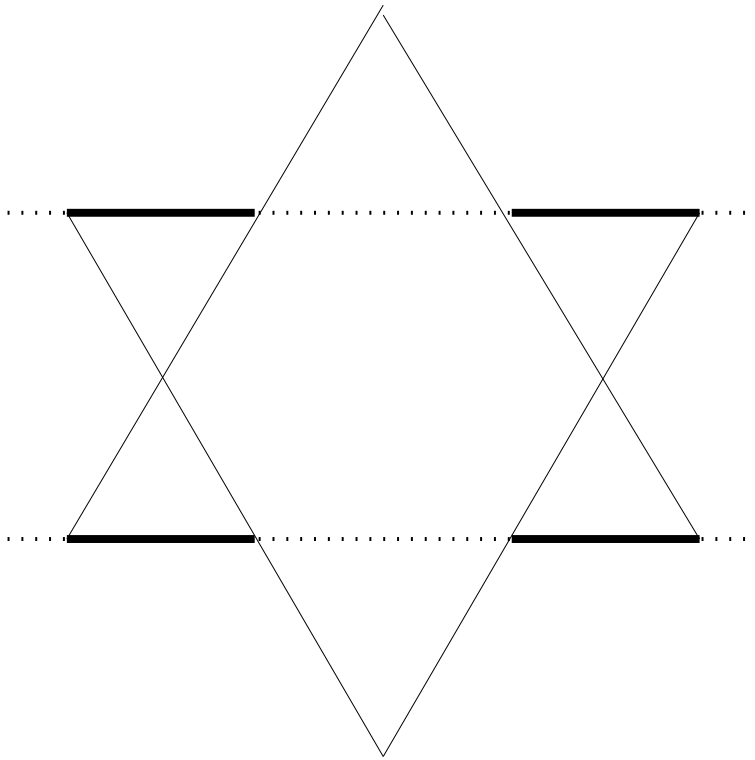


FIG. 3. Mass perturbation to produce M_1 . Bold lines are increased in strength, dotted lines are reduced in strength.

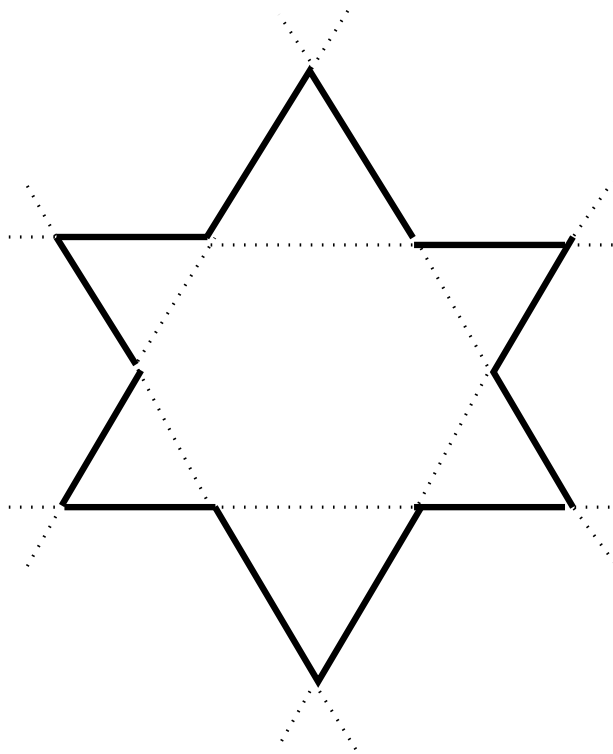


FIG. 4. Mass perturbation to produce M_{12} . Bold lines are increased in strength, dotted lines are reduced in strength.

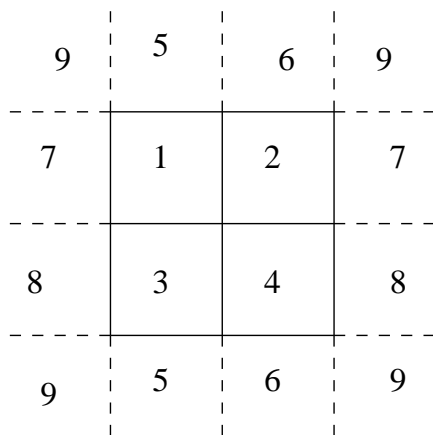


FIG. 5. π -flux phase on square lattice with odd number of sites. Numbers label different squares, each containing $\pi \pm \frac{\pi}{9}$ flux.

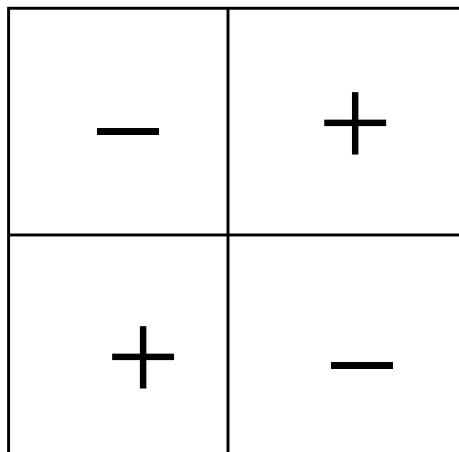


FIG. 6. Enlarged torus to compute wavefunctions.